ULTIMATE SENSITIVITY WITH ISOCAM

B. ALTIERI, L. METCALFE, AND J. BLOMMAERT
ISO Science Centre,ESA Astrophysics Division, VILSPA, P.O Box 50727, E-28080 Madrid, Spain

AND

D. ELBAZ, J.-L. STARCK, AND H. AUSSEL
Service d'Astrophysique, DSM/DAPNIA/CEA-Saclay, F91191 Gif-sur-Yvette Cedex, France

Abstract. We discuss the instrumental factors which constrain the sensitivity limits of the mid-infrared camera (ISOCAM) of ESA's Infrared Space Observatory (ISO). The observing strategy judged to be best suited to faint-source detection is described. A data analysis technique adapted to the extraction of the faintest point-sources is discussed. We report the application of these techniques to an extremely deep mid-IR observation of high redshift gravitationally lensed objects, in two filters, looking through a lensing galaxy cluster.

1. Introduction

To take advantage of the unprecedented mid-IR sensitivity of the ISOCAM instrument on-board the ISO satellite, several deep cosmological or galaxy cluster observations have been performed with the Long Wavelength (LW) channel of ISOCAM. This paper describes the problems related to faint-source detection, the preferred observation strategy, and one of the best adapted algorithms for their detection: PRETI developed at CEA/Saclay. The main difficulty in dealing with ISOCAM faint-source detection is the combined effect of the cosmic ray impacts (glitches) and the signal transient drift behaviour of the LW detector. Once these obstacles are overcome however, results at the fainter limits of the pre-flight expectations for ISOCAM performance are obtained, and these strongly constrain cosmological models.

2. Observations with ISOCAM

The ISOCAM instrument (Cesarsky et al., 1996) was one of the 4 instruments on board ESA's Infrared Space Observatory (ISO) satellite (Kessler et al., 1996). ISOCAM operated in the near- to mid-infrared 2.5-17 μm range. Most of this wavelength range is inaccessible to ground-based instruments due to atmospheric absorption and emission.

The ISOCAM sensitivity was limited by 3 factors:

- the fundamental photon Shot noise and the detector read noise ;
- the signal drifts due to Transients (drifts which occur upon flux changes or following glitches) ;
- the flat-field noise (post-flat-fielding residual variations in responsivity from pixel-to-pixel).

2.1. THE PHOTON SHOT NOISE AND DETECTOR READ NOISE

These are the classical noise sources encountered with all array detectors, and for ISOCAM they both diminish with the square-root of the overall exposure time for any sky pixel. ISOCAM exposures are built up from many detector readouts. Faint-source measurements were accomplished in a rastering (drizzled) mode. The duration of the on-chip integration time was limited by the rate of cosmic ray particle impacts on the detector - the glitch rate. For faint source work the longest on-chip integration time which could be tolerated was used. Typically this was 5 to 10 seconds for the CAM LW detector. A deep faint-source measurement might then accumulate in the region of 1000 to 2000 readouts (5000 to 10000 seconds) observation time for the most deeply sampled sky pixels.

2.2. TRANSIENTS AND GLITCHES

Transient signal drifts occur whenever the detector is exposed to a change in illumination level. These transients affect to some degree all ISOCAM data. For LW, the pixel response to a positive flux change can be decomposed roughly into an initial step-response corresponding to about 60% of what should be the final signal change. This occurs within the 2 first readouts after the flux step - and is followed by a very slow signal increase, with very long time constants when the flux change is small. For faint-source measurements, made typically in rastering mode with just 10 or 15 readouts per raster position (see Section 3.), sources are usually measured close to the initial rising edge of the transient. More on transient behaviour of the detector can be found in Abergel et al. 1998.

The effects of the cosmic ray particle impacts or glitches depend strongly on the signal transient behaviour of the detector. The glitches, depending upon the type of triggering particle, can trigger strong upward or downward excursions of signal which can strongly increase the noise level in the data, and which can conceal or simulate true faint-source detections.

The glitch rate is about 1 per second on the CAM LW detector. It is so large because the detector is large compared to the standard arrays today. This means that, for a typical 5 second on-chip integration, about five particle tracks will occur in the detector. On average each track affects about 8 pixels, so that very roughly about 5% of the detector pixels are contaminated by glitches in each 5 second readout.

Glitches can be divided into 3 families based upon their temporal profile following the triggering particle impact;

- the common glitches, that affect very few readouts and do not introduce signal variations.
- the *faders*, strong glitches followed by a long decaying tail.
- the *dippers*, glitches which suppress the signal by factors up to 20% or more in some cases, and leave long negative tails, in extreme cases lasting hundreds of readouts (and are attributed to heavy-ion impacts).

The glitches are a major constraint on the sensitivity of the LW array. Wherever a glitch occurs at least a few readouts immediately following the impact must be masked out.

The size distribution of glitches does not obviously follow a gaussian distribution. They certainly represent a non-gaussian contribution to the overall noise in the data. This means that the rms of the signal from any given pixel over a period of time yields a value that cannot readily be used to specify the 68% confidence level for source detections on that pixel. I.e. 1-σ (one RMS) does not have the usual statistical significance associated with a gaussian distribution. For more details and glitch characterisations, see Claret et al., 1998 and Dzitko H. et al. 1998

Nevertheless, after appropriate steps have been taken to remove glitch spikes and to restore or suppress the values of distorted signals, the final raster mosaic image can be constructed, and the spatial noise over the image **is** essentially gaussian. Then physically meaningful, conventional, 1-σ sensitivity levels can be defined on the re-constructed image, when the redundancy in the deep raster is high enough. For the deepest rasters, the deepest parts of the field will correspond to sky pixels which have been sampled by something of the order of 100 different detector pixels.

2.3. FLAT-FIELD NOISE

The detector "flat-field" is the map of relative-responses of the detector pixels to a source of uniform brightness-distribution within the field-of-view (FOV). The flat-field can be determined in more than one way, adapted to some extent to the nature of the observation to be corrected. After flat-fielding, the unavoidable residual pixel-to-pixel differences of response are a classical source of additional noise. These pixel-to-pixel response variations contribute a noise term proportional to the accumulated signal, and which therefore has the potential to saturate the S/N after only a few hundred readouts, especially for CAM filters having wavelength ranges in the brighter parts of the Zodiacal light spectrum.

In practice, the effects of this residual flat-field noise can be removed by appropriate filtering of the data, e.g. a 'wide-window' median filterering of the pixel time histories (Altieri et al. 1998a for the method description) or a multi-scale median filtering (PRETI method, see § 4, and Starck et al. 1997 for more details). This follows from the fact that, as stated earlier, CAM exposures are built from many individual readouts. Also, the observation is made in raster mode, so that source detections occur as step functions in the time-history of detector pixels. These "steps" occur as a source comes to rest for a time on a pixel.

If the smoothed time history of the signal from a pixel is fitted and subtracted from the unsmoothed signal, then all background contribution along with residual flat-field induced fluctuations, all long-term signal drifts, and many glitch remnants, are suppressed. What remains are the step-function source detections, plus some residual glitch spikes and dips, and the shot and poisson noise. It must be stressed that this approach is only suitable for application to point-sources, because it attenuates extended source structure. It is also noted that the photometric calibration of point-source measurements must take account of any impacts of the smoothed-baseline subtraction. Careful studies have been, and are being, made of this effect, and an appropriate technical note, prepared by the CAM team at ESA's ISO Science Operations Centre (SOC) in Madrid, is scheduled for placement on the ESA ISO web pages in mid-1998.

Notwithstanding this capacity to remove the effects of the flat-field from faint point-source measurements, it is nonetheless important to flat-field the original data-cube before building the raster mosaic, so that the images suffer only from residual flat-fielding problems. This is so because the flat-field continues, even after filtering of the data, to impact the photometric precision for individual point-source detections.

Flat-fields may be extracted from the calibration libraries used for the ISO Offline Processing Pipeline standard processing. These flat-fields have been measured on the zodiacal light, during in-flight calibration of the instrument, for those CAM filters broad enough to yield sufficient signal. Then for all CAM LW filters and optical configurations, library flat-fields have been derived. These library flat-fields often give very good results and are supplied to all observers along with their data, for standard calibration purposes. But these flat-fields cannot match perfectly the conditions of every observation. One important limitation arises in the fact that, due to some slight jitter in CAM lens wheel positioning, the optical vignetting profile seen by the detector may be slightly different from one observation to the next - so that the flat-field changes slightly, in a systematic way. Improved corrections for this effect are under study. For a description of the ISOCAM flat-field calibration and noise introduced by library flats, we refer to Biviano et al., 1998a and 1998b.

However, for long raster observations on homogeneous flat backgrounds, an optimal flat-field can be built directly from the data. During the faint-source raster, almost all sources remain below the noise level in any one readout. The time history of each pixel is dominated by the constant illumination of the zodiacal background. By assigning a flat-field value to each pixel, equivalent to the median of its values throughout the duration of the raster measurement, one arrives at a flat-field excellently adapted to the particular configuration and measurement in question. Of course, careful judgement must be employed to ensure that the accumulated background signal for the measurement is sufficient to generate a high signal-to-noise flat-field. For the typical faint-source survey filters LW2 and LW3 this is almost always the case.

The flat-field generated in this way is called the *auto* flat in CIA (CAM Interactive Analysis package), see Ott et al., 1996, and the CIA User's Manual for its use (Delaney et al., 1997). This method generally gives much better results than can be obtained using library calibration flat-fields. However, the *auto*-flat may still be perturbed by the transient effects in the pixel histories. A global transient usually occurs throughout an observation following the initial illumination-change on the detector, and glitch induced transients also occur. Therefore a baseline filtering technique such as that described above is extremely beneficial in trying to reach the faintest levels.

3. Observing Strategy

The parameters for a deep ISOCAM LW raster are as follows :

- the central wavelength and width of the filter
- the on-chip integration time: T_{int}
- the Pixel-field-of-view (PFOV) (1.5", 3" or 6" per pixel. 12" was rarely used, and never for faint-source detection.)
- the number of readouts used to build the full exposure: N_{exp}
- the raster step size
- the redundancy (in a single raster + in overlapping rasters) - the number of times each sky pixel was sampled by some detector pixel.

The central wavelength is driven by the scientific requirements of the observation, balanced by considerations of sensitivity achievable in the various configurations. For deep imaging observations, large band-width filters with the highest sensitivity are obviously desirable. Therefore the most used filters for deep imaging (cosmological surveys for instance) were:

- LW2 (5-8.5 μm, reference wavelength 6.7 μm)
- LW3 (12-18 μm, reference wavelength 14.3 μm)
- LW10 (8-15 μm, reference wavelength 12 μm; IRAS filter)

with the reference wavelengths taken from Blommaert et al.(1998), where they are justified.

The trade-off between T_{int} and glitch rate was described in Section 2.1 above, leading to the choice of the largest T_{int} compatible with keeping the glitch rate at an acceptable level. Data with $T_{int} = 20$ seconds would offer extremely favourable read-noise performance, but are almost very difficult to deglitch, so that it was advised early on in the mission not to use this on-chip integration time. However ultra-deep observations of the SSA13 field (22 hours under the japaneese guaranteed time) were taken late in the ISO mission with $T_{int} = 20$ sec., and lead apparently to good results. See Biviano et al. (1998b) for a more quantitative analysis.

As also explained earlier, glitches are also better corrected with higher redundancy rasters.

At 14.3μm, with appropriate filtering of the data to remove the effects of flat-fielding residuals, the dominant noise factor is still related to the high zodiacal background. Photon noise and read-noise levels are comparable, but the glitch induced responsive transients interacting with the relatively high background signal, ensure that optimal performance is achieved by avoiding the $T_{int} = 10$ seconds setting, in favour of $T_{int} = 5$, for LW3.

For LW2 at 6.7μm the $T_{int} = 10.08$ second option was sometimes preferred because of the greater significance of the readout noise at the corresponding lower Zodiacal background levels.

TABLE 1. Noise characteristics

$\lambda(\mu$m)	Integration Time	Dominant noise
6.7 μm	10 seconds	READOUT noise
14.3 μm	5 seconds	PHOTON noise

The choice of the pixel-field-of-view requires a trade-off between the spatial resolution and the sensitivity. A big pixel-field-of-view will give more flux per pixel for a given point source. This implies, in principle, a better

S/N per pixel once the baseline - including the residual flat-fielding noise - has been removed. However, in relatively crowded fields, such as the regions near the centres of galaxy clusters, the map may be affected by confusion of the numerous overlapping sources.

Observers found *qualitatively* that the ultimate sensitivity in uncrowded fields is reached when:

– using the largest $6''$ PFOV
– oversampling the pixels using non-integer raster steps.

And in our observations in crowded fields we found that the ultimate sensitivity may be enabled when:

– using the smaller $3''$ PFOV
– oversampling the pixels using non-integer raster steps.

The final effective pixel size can be as small as $1''$, when using the $3''$ PFOV, but the minimal source separation stays close to the original physical pixel size ($3''$). The spacecraft jitter ($\sim 0.5''$) is still small compared to this pixel size and only marginally extends point sources.

The raster step size must be small enough to allow the largest redundancy within a raster. But the step size must be larger than the FWHM of the PSF, at least in one raster direction, so that the same source does not illuminate the same pixel for successive raster steps. If it does then the baseline removal along the time-axis will more strongly impact source photometry. Dedicated ISO calibration measurements were made during the mission to quantify these effects and technical information notes are in preparation at the ESA ISO Data Centre in Madrid, Spain, complementary to the simulation studies already performed by CEA/Saclay. The number of readouts per raster position need not be much higher than 10. This is so because, as explained in Section 2.2 above, after the initial flux step when a source arrives on a pixel, the signal stabilizes only very slowly. The initial signal step is typically about 60% of the eventual stablized signal difference. During the mission, the practical wisdom was that the slow, asymptotic rise in signal meant that the benefits of keeping the source on one pixel were outweighed by the glitch-rejection benefits derived from moving the source over the array. At the time of writing, after the end-of-mission, the discussion on the best compromise to chose between redundancy and stabilisation is still an open issue.

So finally the main free parameter is the redundancy, i.e. the number of times a sky pixel will be seen by a detector pixel. A high redundancy will reduce the residual flat-fielding noise, especially beneficial if eventually any extended structure is to be examined, and it increases the reliability of source detection.

TABLE 2. Optimum Observing Strategy point source surveys - uncrowded fields

PFOV	6″	
Filter	LW2	LW3 or LW10
N_{exp}	12	20
T_{int}	5 to 10 sec	5 sec
raster step	$\sim 15''$	

TABLE 3. Optimum Observing Strategy point source surveys - crowded fields

PFOV	3″	
Filter	LW2	LW3 or LW10
N_{exp}	12	20
T_{int}	5 to 10 sec	5 sec
raster step	$\sim 15''$	

This kind of observational strategy should also be best suited for deep observation with SIRTF in the future, even if the detector technology is different. In other words, microscanning (making raster steps not corresponding to integer multiples of pixel dimensions) combined with a high redundancy should lead to the best results. Note that this kind of observation strategy was used for the Hubble Deep Field observation with HST, so this technique is more general to deep CCD imaging (in the optical and the IR). We should, of course, bear in mind that the exploration of the ISO data has only really begun, so we must keep an open mind and expect later refinements and refined discussion of these conclusions.

4. Data Reduction using PRETI

4.1. METHOD

The CEA/Saclay team has developed a dedicated technique for data reduction of faint-source rasters: PRETI (Pattern REcognition Technique for ISOCAM data). PRETI is based on the multi-resolution analysis of the cube of data generated by a deep-raster observation, and is described in detail in Starck et al., 1997. Note that this is not the only data reduction

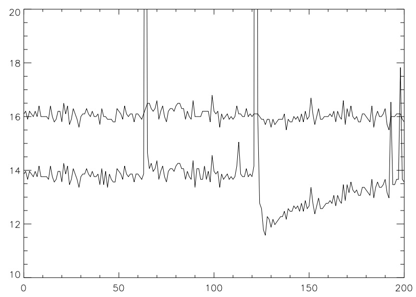

Figure 1. *dipper* glitch good correction by the PRETI method

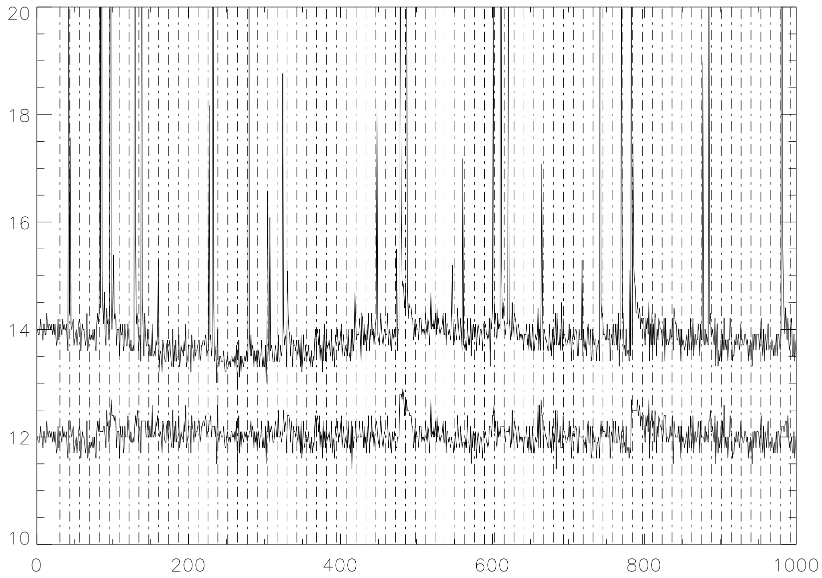

Figure 2. Example of 2 spurious source detections after standard processing

technique for detection of faint sources. Refer to Altieri et al. (1998a), for a description of the other methods developed, or being developed or tested, in the ISOCAM consortium or at the ESA ISO data centre.

PRETI allows the deglitching of the data, by separating the different frequencies of the signal and extracting long glitches using a multi-resolution technique based on the median transform in the temporal history of each pixel.

4.2. RESULTS

One can roughly scale the source sensitivities reached per beam, with the square root of the total integration time, for different observations. The 1σ–1 hour scaled sensitivities reached, with a redundancy of 36 per single raster found in Taniguchi et al., 1997 on the Lockman Hole and Aussel et al, 1998 on the HDF are given in table 4. These deep imaging observations confirmed the very sensitive in-flight performance of ISOCAM.

TABLE 4. 1 σ – 1hour sensitivity

Filter	LW2	LW3
Theoretical	10 μJy	40 μJy
Effective	15 μJy	40 μJy

As the algorithms involve filtering of signals, and as glitches introduce a non-gaussian noise, the best way to determine the effective sensitivity limit is to build simulated data by introducing false sources (with transients and PSF included) into a real data set (hence with a real distribution of glitches)

Simulations indicate that the completeness, for HDF-like observations with 1.8 hours cumulative dwell-time per sky pixel is as reported in table 5.

TABLE 5. completeness

Filter	LW2	LW3
95%	50 μJy	100 μJy
80%	40 μJy	90 μJy

Aperture photometry must be performed on ISOCAM faint sources. It has been used early by Goldschmidt et al. (1997) on the ISOCAM observations of the HDF, and was shown by Aussel et al. (1998), through various simulations, to be linear down to the faintest fluxes. However at the faint end tail of the flux distribution the aperture photometry starts deviating positively from linearity due to the glitch pollution (say sources detected at 4σ or below). Due to wide PSFs with ISOCAM, the aperture photometry consists in computing the source flux within a circular aperture of about the size of the FWHM ($5''$ to $7''$) and correcting for flux loss in the wings by appropriate factors given by calibration stars observed with the same observational settings. Typically, 55% and 65% of the energy are encircled in an aperture diameter of $7''$ in LW3 and LW2 respectively. Other types of photometry such as Kron-like elliptical fitting, in SExtractor (Bertin & Arnouts, 1996) or 'full object' wavelet photometry are non-linear at faint fluxes.

5. Ultimate CAM rasters: application to a deep crowded field

In order to push ISOCAM to the limits, both in terms of sensitivity and spatial resolution, we performed a series of observations which we refer to as the *ultimate raster* and which was targeted to obtain some of the deepest ISOCAM images. This was implemented within ESA SOC guaranteed time, as a follow-up to an ESA Guaranteed Time programme using gravitational lensing clusters to probe the more distant background (Metcalfe et al., 1997 and 1999, Altieri et al., 1998b) and was allocated one full ISO revolution, which amounts to 16 hours of science time. The target chosen was Abell 2390, a very rich galaxy cluster where many mid-IR sources were expected to fall in a small area, with the source counts augmented by the gravitational lensing amplification of this famous lensing cluster. (Mc Breen & Metcalfe, 1987, Paczynski B., 1986)

Optimum spatial resolution being essential in this case, the $3''$ PFOV was chosen. Emphasis was put on high redundancy by performing four 10x10 rasters in each of the 2 filter bands LW2 and LW3, leading to a redundancy factor of 400 in each filter in the central part of the covered area. The 4 rasters were slightly offset relative to each other to make the best use of the drizzling technique. $T_{int} = 5$ sec was chosen, to keep each individual raster to a *reasonable time* of 2 hours, for convenience in achieving optimum scheduling in the low-glitch-rate time near orbital apogee. Finally the minimum recommended step size (minimum for the data reduction filtering strategy preferred) of $7''$ was taken - this being very close to the FWHM of the LW3 PSF. This step-size allows an extremely high redundancy in each individual raster (100 in the central part).

From the discussion in the sections above, it is seen that this represents the optimum faint-source observing strategy interpreted for a relatively crowded field and adapted to the scheduling constraints of these very, very long cumulative exposures. Table 6 summarises the observation strategy taken for the *ultimate* CAM rasters.

This approach yielded excellent scientific results very close to the limits found with surveys at $6''$ PFOV, reported in tables 4 and 5, but deeper when the gravitational magnification is taken into account. See fig. 3 for the ultra-deep LW3 map through the cluster-lens Abell 2390, where almost all sources are lensed distant objects (Altieri et al., 1998c, 1988d).

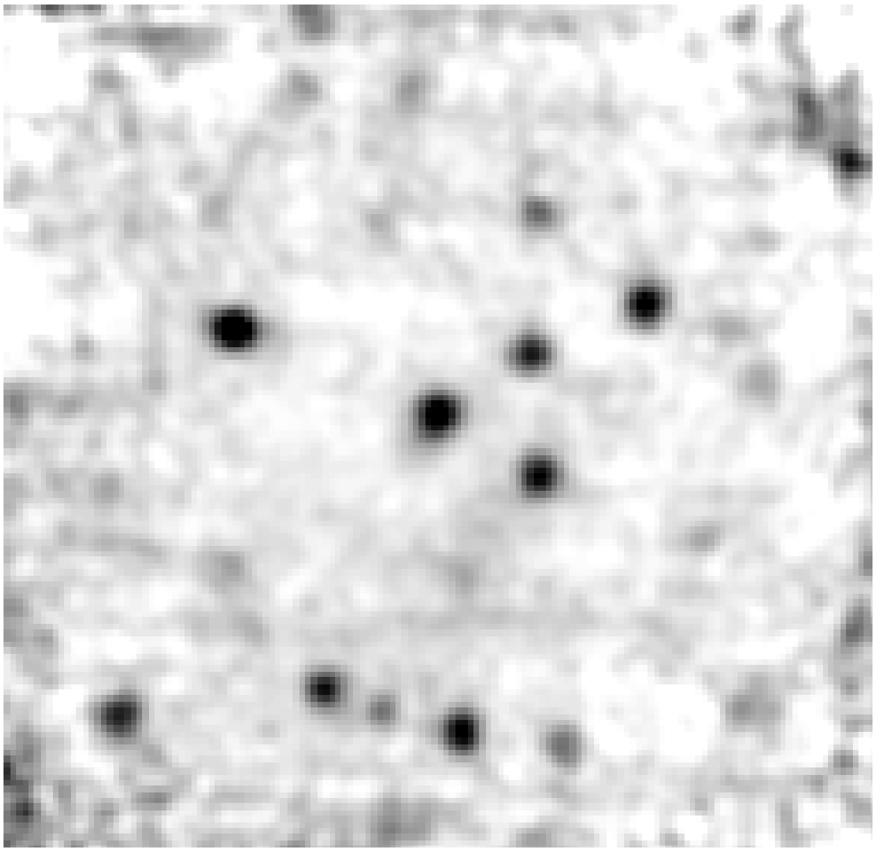

Figure 3. Ultra deep map through the Abell 2390 cluster-lens

TABLE 6. Ultimate CAM rasters

PFOV	3″	
Filter	LW2	LW3
N_{exp}	13	13
T_{int}	5 sec	5 sec
raster step size	$\sim 7''$	
raster size	4 10x10 rasters	
maximal redundancy	400	

6. Conclusion

Deep imaging observations with ISOCAM confirmed the excellent in-flight performance of the ISOCAM instrument, which matched the best pre-flight hopes. The faintest ISOCAM flux levels claimed are : in the $6''$ PFOV, around 50μJy at 14.3μm on the ISOCAM observations of HDF (Rowan-Robinson et al., 1997; Aussel et al., 1998) and about 30μJy at 6.7μm on the Lockman Hole (Taniguchi et al, 1997), about 4 orders of magnitudes below IRAS, and, in the $3''$ PFOV about 30μJy at 14.3μm on Abell 2390 with the help of gravitational lensing.

One of the best methods for data reduction, adapted to detect faint point-sources in deep raster observations with the ISOCAM LW detector, is the PRETI method, developed by Starck et al.

Acknowledgements

The ISOCAM data presented in this paper was analysed using "CIA", a joint development by the ESA Astrophysics Division and the ISOCAM Consortium. The ISOCAM Consortium is led by the ISOCAM PI, C. Cesarsky, Direction des Sciences de la Matiere, C.E.A., France.

References

Abergel, A., et al., 1998, this volume

Altieri, B. et al., 1998a, 'The ISOCAM Faint sources report', ESA/SSD, ISO WEB Explanatory library.

Altieri, B., Metcalfe, L., et al., 1998b, in *The Young Universe*, Monteporzio conference proceedings, in press, astro-ph/9803155

Altieri, B., Metcalfe, L., et al., 1988c, ESA SP-431 conf. proceedings, "NGST workshop: Science Drivers and Technological Challenges", astro-ph/9808131

Altieri, B., Metcalfe, L., Kneib, J.-P., et al., 1998d, A&A letter, submitted, astro-ph/9810480.

Aussel, H., Cesarsky, C., Elbaz, D., Starck J.-L., 1998, A&A in press, astro-ph/9810044

Bertin, E. & Arnouts, S., 1996, A&A, 177, 393

Biviano, A., et al., 1998a, 'ISOCAM Flat-field calibration report', ESA/SSD, (ISO WEB explanatory library)

Biviano, A., 1998b, 'The ISOCAM Calibration Error Budget Report', version 3.1, (ISO WEB explanatory library)

Blommaert, J., Metcalfe, L., Altieri, B., et al., 1998, this volume

Boulade, O. & Gallais, P., 1998, ISOCAM Detectors: an Overview, this volume

Cesarsky, C.J., et al. 1996, A&A 315, L32

Claret, A., et al, 1998, this volume

Delaney, M. et al, 'ISOCAM Interactive Analysis User's Manual, Version 2.0, reference SAI-96-5226/Dc

Dzitko, H., et al, 1998, this volume

Goldschmidt, P., Oliver, S., Serjeant, S., et al, 1997, MNRAS, 289, 465

Kessler, M.F., et al. 1996, A&A 315, L27

Ott, S., et al., 1997, "Design and implementation of CIA, the ISOCAM interactive analysis system", ASP conference series vol.125

Mc Breen, B., Metcalfe, L., 1987, Nature, Vol.330, p348
Metcalfe, L., Altieri, B., et al., 1997, "ISO Mid-IR observations of Abell 370" in *Extragalactic Astronomy in the Infrared*, Edt Frontieres, G. Mamon, astro-ph/9803174
Metcalfe, L., Altieri, B., Kneib., J.-P. et al., 1999, under preparartion.
Paczynski, B., 1986, Astrophys. J., 301, 503-516.
Rowan-Robinson, M., Mann, R., Oliver, S., et al., 1997, MNRAS, 289, 490
Starck, J.-L., Aussel, H., Elbaz, D., 1997, in *Extragalactic Astronomy in the Infrared*, Ed. Frontières, Mamon G.A.
Taniguchi, Y., Cowie, L., Sato, Y. et al., 1997, A&A, 329, L9